The HKU Scholars Hub   The University of Hong Kong   香港大學學術庫

Title	Evaluation of radiation dose and image quality for the Varian cone beam computed tomography system
Author(s)	Cheng, HCY; Wu, VWC; Liu, ESF; Kwong, DLW
Citation	International Journal of Radiation Oncology Biology Physics, 2011, v. 80 n. 1, p. 291-300
Issued Date	2011
URL	http://hdl.handle.net/10722/139117
Rights	

Evaluation of radiation dose and image quality for the Varian cone beam computed tomography system

Harry C. Y. Cheng, M.Sc.,* † Vincent W. C. Wu, Ph.D.,‡ Eva S. F. Liu, M.Eng.,† and Dora L. W. Kwong, M.D.*

*Department of Clinical Oncology, The University of Hong Kong, Hong Kong SAR, China; †Department of Clinical Oncology, Queen Elizabeth Hospital, Hong Kong SAR, China; ‡Department of Health Technology and Informatics, The Hong Kong Polytechnic University, Hong Kong SAR, China

Abstract

Purpose

To compare the image quality and dosimetry on the Varian cone beam computed tomography (CBCT) system between software Version 1.4.13 and Version 1.4.11 (referred to as "new" and "old" protocols, respectively, in the following text). This study investigated organ absorbed dose, total effective dose, and image quality of the CBCT system for the head-and-neck and pelvic regions.

Methods and Materials

A calibrated Farmer chamber and two standard cylindrical Perspex CT dosimetry phantoms with diameter of 16 cm (head phantom) and 32 cm (body phantom) were used to measure the weighted cone-beam computed tomography dose index (CBCTDI$_w$) of the Varian CBCT system. The absorbed dose of different organs was measured in a female anthropomorphic phantom with thermoluminescent dosimeters (TLD) and the total effective dose was estimated according to International Commission on Radiological Protection (ICRP) Publication 103. The dose measurement and image quality were studied for head-and-neck and pelvic regions, and comparison was made between the new and old protocols.

Results

The values of the new CBCTDI$_w$ head-and-neck and pelvic protocols were 36.6 and 29.4 mGy, respectively. The total effective doses from the new head-and-neck and pelvic protocols were 1.7 and 8.2 mSv, respectively. The absorbed doses of lens for the new 200° and old 360° head-and-neck protocols were 3.8 and 59.4 mGy, respectively. The additional secondary cancer risk from daily CBCT might be up to 2.8%.

Conclusions

The new Varian CBCT provided volumetric information for image guidance with acceptable image quality and lower radiation dose. This imaging tool gave a better standard for patient daily setup verification.

Author Keywords

Cone beam computed tomography; Image-guided radiation therapy; Patient dose; On-board imager; Thermoluminescence dosimeters

Introduction

The advent of three-dimensional (3D) cross-sectional imaging, 3D conformal radiotherapy and intensity-modulated radiation therapy (IMRT) has been shown to allow dose escalation and reduce normal tissue toxicity, thus improving local control and disease-free survival [1], [2], [3] and [4]. The planning target volume (PTV) of many advanced head-and-neck cancers is close to many organs at risk (OARs). A typical example is the radiotherapy of advanced stages of nasopharyngeal carcinoma (NPC), in which the close proximity of the brainstem, spinal cord, and optic structures to the PTV, requires highly conformal coverage with steep dose gradients. Conventional methods of treatment verification have been performed by the acquisition of two-dimensional (2D) megavoltage (MV) images through verification films or electronic portal imaging devices (EPID), which demonstrate bony anatomical landmark but do not discriminate the contrast of soft-tissue structures such as muscle and fat. The disadvantage of using MV images over kilovoltage (kV) images is the inherent decrease in soft-tissue contrast because of the low Z-dependence at high energies [5], [6] and [7].

Image-guided radiation therapy (IGRT) with on-board kV cone beam computed tomography (CBCT) system installed on linear accelerators is becoming more popular in radiation therapy in the past few years [8], [9], [10] and [11]. This system consists of a kV x-ray source with an opposed amorphous silicon (aSi) or selenium flat-panel detector mounted onto the gantry of the linear accelerator. The CBCT system shares a common axis of rotation with the MV treatment source. Rotation of the CBCT system around the patient produces a series of computed tomography (CT) images that can create a set of volumetric 3D data.

The CBCT provides accurate information on 3D volumetric soft tissue and bony structure information about the patient's anatomy on a daily basis and is essential for adaptive radiation therapy (ART) [8], [12], [13] and [14]. Compared with 2D localization based on only bony landmarks using either on-board imager (OBI) or EPID, the CBCT is more accurate because it is possible to localize soft tissues such as targets and OARs in 3D images (15). Through use of software for image registration operated manually or automatically, geometric errors of the patient setup between the CBCT images and the planning CT can be found. This positional error can then be corrected by applying shift of the treatment couch. Although setup margin is usually added to the PTV and OAR according to the ICRU 62 (16), it is essential to minimize the geometric uncertainty within the setup margin with the help of imaging devices such as CBCT, OBI, or EPID. These ensure that accurate dose is delivered to the targets while the doses to the OARs are within their tolerance.

The first generation of the CBCT system of the Varian linear accelerator (Varian Medical Systems, Palo Alto, CA) operates the CBCT through 360° scanning. The 2008 Varian upgraded software of acquiring CBCT images has three improved features aiming at reducing patient dose. The first improvement is reducing the volume of the patient receiving radiation by adjusting the collimator blades that control the size of the kV x-ray beam. Radiation therapists can adjust the x-ray field size when acquiring CBCT images to reduce the cranio-caudal extent of the CBCT scan. Reducing the cranio-caudal extent of the scan not only reduces the irradiated volume of the patient but also improves the image quality of the CBCT by reducing scattered radiation contributing to the reconstructed images. The second improvement is introducing various x-ray scanning protocols that best match the clinical task with the minimum radiation dose. For many treatment sites especially in the head-and-neck region, low-dose CBCT is sufficient to verify the treatment position for patients (17). However, when soft tissue contrast is required for positioning, such as in lung and prostate cancers, the scanning protocol with higher dose can be selected, and this helps in visualizing the tumor for accurate positioning. The third improvement is selecting the direction of the kV beam to avoid sensitive structures such as the lens in the head-and-neck region. The

upgraded version of the CBCT software allows a choice of either 200° or 360° scanning for image acquisition. A 200° scanning for image acquisition is useful for a head-and-neck cancer patient treated in a supine position. The kV x-ray traverses from lateral and posterior directions of the skull. Therefore the lenses receive only the exit radiation dose, which is much lower than the entrance dose when the beam is incidence from anterior.

The aim of this study is to evaluate the kV imaging dose of the most common head-and-neck and pelvic protocols for the CBCT system with software Version 1.4.13 (referred to as "new" protocol in the following text) provided by the vendors that are in current clinical use and compare them with the previous software Version 1.4.11 (referred to as "old" protocol in the following text). It is important to quantify the effective dose and the additional risk of inducing secondary cancers from kV imaging for patients undergoing radiation therapy. The image quality is also compared between the two imaging scanning protocols. This study will give useful information to clinicians on radiation dose and image quality of CBCT and help in making decision regarding use of CBCT in IGRT.

Methods and Materials

Equipment

The Varian Clinac 23EX linear accelerator with integrated OBI system was used. This OBI system includes a kV x-ray tube (Varian Medical Systems, Palo Alto, CA) with nominal x-ray tube voltage of 150 kV and a 30 cm × 40 cm aSi flat-panel detector (Varian Medical Systems, Palo Alto, CA) directly opposite. It is mounted perpendicular to the treatment head on the gantry of the linear accelerator using a robotic arm (Exact).

Image acquisition

Two scanning modes are available in this system: full-fan and half-fan. For the full-fan mode, the largest reconstructed field of view (FOV) is a circle of 25 cm diameter with a 18-cm length in volume. This mode is used for visualizing small anatomical sites such as the head-and-neck region or small soft-tissue organs such as the prostate. For the half-fan mode, the aSi detector is shifted of 14.8 cm in a perpendicular direction to the kV beam axis to increase the scanning area and the maximum reconstructed FOV is a circle of 45 cm diameter and 18 cm in length [18] and [19]. This mode is commonly used in the regions of pelvis, abdomen, or thorax. A bowtie filter should be used to reduce skin dose to the patients as well as possibility of detector saturation [20] and [21]. There are two types of bowtie filters, full-fan and half-fan, which are used with the full-fan and half-fan scanning modes, respectively. To acquire a set of CBCT, the kV source is rotated either 200° (from 90° to 290°) or 360° around the patient who lies in the treatment position on the treatment couch, and it takes approximately 35 to 60 s. During scanning, 360 to 720 image projections of the patient can be acquired. In this study, the default settings of 360 and 655 image projections were used for the scanning protocols with 200° and 360°, respectively. These images were reconstructed to produce 3D images with better volumetric anatomical information. The scanning protocols for this study are shown in Table 1.

Table 1. Scanning protocol of the new and old cone beam computed tomography (CBCT) systems

	New (Version 1.4.13)	Old (Version 1.4.11)	New (Version 1.4.13)	Old (Version 1.4.11)
	Head	Head	Pelvis	Pelvis
X-ray voltage (kVp)	100	125	125	125
X-ray current (mA)	80	80	80	80
X-ray ms (ms)	25	25	13	25
Gantry rotation range (degree)	200	360	360	360
Number of projections	360	655	655	655
Exposures (mAs)	720	1,300	680	1,300
Fan type	Full	Full	Half	Half
Default pixel matrix	384×384	512×512	384×384	512×512
Longitudinal extent (cm)	18	15.5	18	13.7
FOV (cm)	25	25	45	45
Slice thickness (mm)	2.5	2.5	2.5	2.5

Dosimetry of kV photon

According to the AAPM TG61 protocol, a 0.6-cc Farmer-type ionization chamber (PTW TW30010, Freiburg, Germany) and an electrometer (PTW Unidos, Freiburg, Germany), with air kerma calibration factor, N_k, traceable to national standard (Physikalisch-Technische Bundesanstalt, Braunschweig, Germany) were used to determine the absorbed dose to water at the phantom surface (z_{ref} = 0) (22). The protocol recommended that the beam qualities were characterized by the determination of the first half-value layer (HVL) of aluminum (99.9 %) in narrow beam so as to eliminate the effect of electron contamination. The Farmer-type ionization chamber and the attenuator were placed at 100 cm and 50 cm from the source respectively. The beam with a field of 4 ×4 cm was used to determine the HVL (22). With Bowtie filter, the HVLs for the beams of 100 kVp and 125 kVp were found to be 5.0 mm Al and 6.1 mm Al, respectively.

CT dose index of CBCT

Although CBCT has a broad beam characteristic, computed tomography dose index (CTDI) is an appropriate approach for dose reporting if a small and ubiquitous ionization chamber such as 0.6 cc Farmer-type ionization chamber was used to measure the central and peripheral doses in the phantom [18] and [23]. The dose reduction at the periphery and the maximum dose at the central in the longitudinal dose profile were found [24] and [25]. This was attributable to the reduced scatter radiation near the edge of the FOV and the divergent beam in the CBCT (25). Therefore, the measured dose in this study represented the highest dose at the isocenter. It might be inappropriate to use a 100 mm pencil chamber to measure the CBCT dose since it is designed for narrow beam and single slice fan-beam dose measurement. Therefore, the pencil chamber is not suitable for measurement of a point dose. For the measurement of standard CT dosimetry, a 16-cm-diameter head and a 32-cm-diameter body standard Perspex CT dosimetry phantoms (length, 15 cm) were used to measure the dose for the regions of head and pelvis respectively. At least three readings were collected to obtain an average value.

Many authors have recently adopted a concept used in conventional CT called the weighted CT dose index (CTDI$_w$) to estimate the dose of CBCT, which is called as weighted cone beam CTDI (CBCTDI$_w$) and defined as follows (18):

$$CBCTDI_w = (1/3)D_0 + (2/3)\overline{D}_p \qquad (1)$$

where

D$_0$ is the central axis dose and is weighted by 1/3 and

$\overline{D}_p$ is the mean peripheral dose in the phantom at 0°, 90°, 180° and 270° around the gantry at 1 cm from the surface and is weighted by 2/3.

In this study, the concept of the CTDI$_w$ was adopted and CBCTDI$_w$ was estimated for different protocols.

Thermoluminescence dosimeters dosimetry

Thermoluminescence dosimeters (TLDs)-100H chips (Thermo Scientific, Erlangen, Germany), made of LiF:Mg,Cu,P, were used to measure the absorbed dose of a female anthropomorphic phantom (RANDO phantom, The Phantom Laboratory, Salem, NY) for this study. The advantages of the relatively new TLD-100H over the traditional TLD-100 material include higher sensitivity, lower fading rate, and more flat energy response (26). To reduce dose response with energy, the TLD-100H was calibrated and used at one beam quality. A total of 154 TLD chips were used in this study and were divided into two sets. The first and the second sets of TLD were irradiated respectively by 100 kVp and 125 kVp x-ray generated from the OBI system with the bowtie filter. The TLDs with reproducibility within ±3% were selected for calibration and subsequent measurements under three exposures. Each TLD-100H chip was then individually calibrated on the surface of a solid water phantom (Gammex RMI, Middleton, WI) against the absorbed dose determined by the 0.6-cc Farmer-type ionization chamber in air. All TLDs were irradiated three times to assign an individual sensitivity coefficient for the entire study.

The positions of TLDs in the RANDO phantom were based on the 2007 recommendations of the International Commission on Radiological Protection (ICRP) Publication 103 (27). The TLDs were also placed over the eye to estimate the dose to the lens of the eye and other major organs or tissues such as gonad, breast, and bone marrow in the body. Besides, it is noted that the radiation dose to some OARs such as lens, retina, optic nerve, brainstem, and spinal cord in the head-and-neck region may be affected by the position of isocenter for the new 200° head-and-neck scanning protocol. The absorbed doses of these OARs were measured using TLD and three sets of measurement with different isocenters were performed. The isocenters were placed at the center of the head, 4 cm anterior and posterior to the center of the head respectively. The effective dose of the body was calculated according to the ICRP 103 recommendations as follows:

$$E = \sum_T w_T \sum_R w_R D_{T,R} \qquad (2)$$

where

w_R is the radiation weighting factor;

w_T is the tissue weighting factor for tissue T and $\sum w_T = 1$;

$D_{T,R}$ is the mean absorbed dose from radiation R in a tissue or organ T.

Assessment of image quality

The images of CBCT were exported to the Eclipse treatment planning system (TPS) (Varian Medical Systems, Palo Alto, CA) for viewing and assessment of image quality. The image quality was checked against the scanning protocols listed in Table 1. High-contrast spatial resolution, low-contrast sensitivity, image noise, and contrast-to-noise ratio (CNR) were studied using a 20-cm-diameter Catphan 504 phantom (The Phantom Laboratory, Salem, NY) with different inserts. The phantom was aligned with the isocenter of the CBCT. The CTP528 module with 1 to 21 line pairs per cm (lp/cm) was used to study the high-contrast spatial resolution. For the low-contrast sensitivity test, the CTP515 module with three groups of variable size objects with nominal 0.3%, 0.5% and 1.0% contrast levels was used. For each contrast level there are nine cylindrical objects with diameters of 2 to 15 mm. Image noise was measured by the CTP486 module which contains uniform material with CT number (20 Hounsfield Unit (HU)) within 2% of water's density. The CTP404 module with seven high-contrast sensitometric targets was used to study the CNR performance of different scanning protocols of CBCT. For each CBCT, a squared region of interest (ROI) of 0.16 cm2 was outlined for each of the different electron density inserts to measure the mean and standard deviation (noise) in HU values. These inserts are air (−1,000 HU), PMP (−200 HU), low-density polyethylene (LDPE; −100 HU), water (0 HU), polystyrene (−35 HU), acrylic (120 HU), Delrin (340 HU), and Teflon (990 HU). The CNR was calculated as:

$$CNR = \frac{\left|\overline{P}_{ROI,insert} - \overline{P}_{ROI,background}\right|}{\sqrt{\sigma^2_{ROI,insert} + \sigma^2_{ROI,background}}} \qquad (3)$$

where $\overline{P}_{ROI,insert}$ and $\overline{P}_{ROI,background}$ refer to the mean pixel values and $\sigma_{ROI,insert}$ and $\sigma_{ROI,background}$ refer to the standard deviations in a squared ROI inside the insert and the background of the module, respectively [28], [29] and [30]. To normalize image quality to the radiation dose to the patient, the figure of merit (FOM), which is independent of dose and can be used as an indicator of improvement in image quality per radiation risk to the patient, for each protocol is calculated as follows [31], [32] and [33]:

$$FOM = \frac{CNR^2}{CTDI_w} \qquad (4)$$

Results

CBCTDI$_w$ measurement

Table 2 shows the CBCTDI$_w$, measured using the 0.6 cc Farmer-type ionization chamber in either the 16-cm or 32-cm diameter CTDI phantom according to the scanning protocols. The CBCTDI$_w$ is an imperative and objective indicator of the average radiation dose within the CTDI phantom. For the head-and-neck region, the values of CBCTDI$_w$ of the new and old protocols were 36.6 and 116.8 mGy, respectively. For the normalized CBCTDI$_w$, the new and old protocols were 5.1 mGy/ 100 mAs at 100 kV with 200° scanning and 9.0 mGy/ 100 mAs at 125 kV with 360° scanning respectively. The values of CTDI at 0° position for the new 200° and the old 360° head-and-neck protocols were 12.9 and 116.1 mGy, respectively. For the half-fan scan of the pelvic region, the new low-dose pelvic protocol with smaller exposure generated the CBCTDI$_w$ of 29.4 mGy and the old pelvic protocol delivered 58.2 mGy. The normalized CBCTDI$_w$ of the new and old protocols were 4.3 mGy/100 mAs at 125 kV and 4.5 mGy/100 mAs at 125 kV, respectively.

Table 2. CBCTDI$_w$ of the new and old scanning protocols

	New (Version 1.4.13)	Old (Version 1.4.11)	New (Version 1.4.13)	Old (Version 1.4.11)
	Head	Head	Pelvis	Pelvis
CBCTDI$_w$ (mGy)	36.6 $\pm$ 0.8	116.8 $\pm$ 3.3	29.4 $\pm$ 0.4	58.2 $\pm$ 1.4
CTDI at center (mGy)	38.1 $\pm$ 0.1	125.6 $\pm$ 0.4	20.2 $\pm$ 0.0	40.5 $\pm$ 0.1
CTDI at 90° (mGy)	32.4 $\pm$ 0.1	111.6 $\pm$ 0.3	33.5 $\pm$ 0.1	65.3 $\pm$ 0.4
CTDI at 180° (mGy)	55.9 $\pm$ 0.2	111.1 $\pm$ 0.3	34.2 $\pm$ 0.0	68.5 $\pm$ 0.1
CTDI at 270° (mGy)	41.9 $\pm$ 0.2	110.7 $\pm$0.4	34.2 $\pm$ 0.0	67.0 $\pm$ 0.2
CTDI at 0° (mGy)	12.9 $\pm$ 0.0	116.1 $\pm$ 0.7	34.1 $\pm$ 0.0	67.7 $\pm$ 0.1
Normalized CBCTDI$_w$ (mGy/100 mAs)	5.1 $\pm$ 0.1	9.0 $\pm$ 0.3	4.3 $\pm$ 0.1	4.5 $\pm$ 0.1

TLD dose in the RANDO Phantom

The average organ doses and the effective doses of the RANDO Phantom measured by TLD for the head-and-neck and pelvic regions are shown in Table 3. The organ dose and the total effective dose from the new 200° scanning protocol were lower than those from the old 360° scanning protocol. The anterior located structures such as lens, retina, and optic nerve for the new scanning protocol received lower dose than the old scanning protocol. The absorbed doses to lens, retina, and optic nerve for the new scanning protocol were 3.8, 9.0, and 10.5 mGy, respectively, whereas for the old scanning protocol the absorbed doses to lens, retina, and optic nerve were 59.4, 69.5, and 60.2 mGy, respectively. The absorbed doses of salivary gland, which was newly recommended by ICRP 103, were 6.0 and 13.0 mGy for the new and old scanning protocols, respectively. The total effective dose from the new 200° scanning protocol was 1.7 mSv, whereas that from the old 360° scanning protocol was 9.4 mSv. The tissues or organs which were not inside the irradiated field received much lower dose, which was primarily contributed from scattered radiation. The skin dose for the new protocol was 4.5 mGy, which was much lower than that of the old protocol (16.8 mGy).

Table 3. Summary of absorbed dose (mGy) and effective dose (mSv) from cone beam computed tomography (CBCT) measured by thermoluminescent dosimeters (TLD) in the RANDO phantom

Organ/tissue	New (Version 1.4.13) Head Absorbed dose (mGy)	Old (Version 1.4.11) Head Absorbed dose (mGy)	Head Dose ratio (New version/ old version)	New (Version 1.4.13) Pelvis Absorbed dose (mGy)	Old (Version 1.4.11) Pelvis Absorbed dose (mGy)	Pelvis Dose ratio (New version/ old version)
Gonad	0.04 ± 0.00	0.20 ± 0.02	0.19	11.66 ± 0.30	22.11 ± 0.47	0.53
Bone marrow	0.02 ± 0.00	0.08 ± 0.01	0.26	14.59 ± 0.17	28.68 ± 0.70	0.51
Colon	0.05 ± 0.00	0.22 ± 0.02	0.24	6.45 ± 0.11	12.50 ± 0.22	0.52
Lung	0.51 ± 0.00	2.56 ± 0.07	0.20	0.25 ± 0.01	0.50 ± 0.01	0.51
Stomach	0.07 ± 0.00	0.43 ± 0.02	0.16	1.35 ± 0.03	2.60 ± 0.06	0.52
Bladder	0.02 ± 0.00	0.13 ± 0.02	0.14	30.37 ± 0.54	59.35 ± 1.27	0.51
Breast	0.18 ± 0.01	1.35 ± 0.08	0.14	0.34 ± 0.01	0.70 ± 0.03	0.49
Liver	0.08 ± 0.00	0.43 ± 0.01	0.19	1.41 ± 0.02	2.70 ± 0.10	0.52
Esophagus	0.90 ± 0.02	3.82 ± 0.29	0.24	0.17 ± 0.01	0.36 ± 0.01	0.48
Thyroid	13.85 ± 0.16	93.39 ± 3.90	0.15	0.11 ± 0.00	0.22 ± 0.00	0.51
Skin	4.46 ± 0.04	16.84 ± 0.64	0.26	10.54 ± 0.29	20.56 ± 1.05	0.51
Bone surface	0.02 ± 0.00	0.09 ± 0.01	0.23	20.83 ± 0.25	40.76 ± 1.01	0.51
Brain	4.97 ± 0.09	20.32 ± 0.47	0.24	0.04 ± 0.00	0.08 ± 0.00	0.58
Salivary gland	6.00 ± 0.12	13.00 ± 0.26	0.46	0.20 ± 0.01	0.25 ± 0.02	0.80
Remainder organ						
Adrenals	0.07 ± 0.00	0.34 ± 0.02	0.22	2.03 ± 0.05	3.92 ± 0.06	0.52
Small intestine	0.05 ± 0.00	0.28 ± 0.01	0.17	3.63 ± 0.07	6.93 ± 0.20	0.52
Kidney	0.07 ± 0.00	0.29 ± 0.02	0.23	2.85 ± 0.06	5.46 ± 0.10	0.52
Muscle	14.11 ± 0.13	27.01 ± 4.82	0.52	12.77 ± 0.29	25.31 ± 0.58	0.50
Pancreas	0.07 ± 0.00	0.42 ± 0.02	0.17	1.45 ± 0.02	2.81 ± 0.05	0.52
Spleen	0.09 ± 0.00	0.43 ± 0.03	0.22	1.39 ± 0.06	2.65 ± 0.15	0.52
Thymus	2.68 ± 0.03	12.41 ± 0.66	0.22	0.11 ± 0.00	0.22 ± 0.00	0.49
Lens	3.79 ± 0.07	59.38 ± 0.84	0.06	0.08 ± 0.00	0.15 ± 0.00	0.54
Retina	9.01 ± 0.17	69.52 ± 0.99	0.13	0.06 ± 0.00	0.11 ± 0.00	0.55
Optic nerve	10.48 ± 0.19	60.24 ± 0.85	0.17	0.05 ± 0.00	0.09 ± 0.00	0.56
Optic chiasma	15.92 ± 0.21	59.46 ± 0.59	0.27	0.05 ± 0.00	0.09 ± 0.00	0.58
Pituitary gland	13.41 ± 0.17	50.64 ± 0.51	0.26	0.05 ± 0.00	0.09 ± 0.00	0.56
Brainstem	17.87 ± 0.29	57.17 ± 1.13	0.31	0.06 ± 0.00	0.10 ± 0.00	0.59
Spinal cord	14.40 ± 0.12	39.94 ± 0.90	0.36	7.08 ± 0.21	13.82 ± 0.00	0.51
Rectum	0.03 ± 0.00	0.11 ± 0.01	0.30	22.75 ± 0.55	46.48 ± 1.07	0.49

Organ/tissue	New (Version 1.4.13) Head Absorbed dose (mGy)	Old (Version 1.4.11) Head Absorbed dose (mGy)	Head Dose ratio (New version/old version)	New (Version 1.4.13) Pelvis Absorbed dose (mGy)	Old (Version 1.4.11) Pelvis Absorbed dose (mGy)	Pelvis Dose ratio (New version/old version)
Heart	0.26 ± 0.00	1.54 ± 0.05	0.17	0.33 ± 0.00	0.66 ± 0.02	0.51
Total effective dose (mSv)	1.65 ± 0.01	9.39 ± 0.16	0.18	8.21 ± 0.04	16.00 ± 0.11	0.51

Table 4 illustrates the TLD absorbed dose of major OARs in the head-and-neck region delivered by the new 200° head-and-neck protocol with different locations of the isocenter. The absorbed dose of lens and retina for the isocenter at 4 cm anterior to the center of the head were 13.0 and 13.3 mGy, respectively, whereas those for the isocenter at the center of the head were 3.8 and 9.0 mGy, respectively. The absorbed dose to the lens and retina were further reduced to 2.6 and 5.0 mGy respectively if the isocenter was shifted 4 cm posteriorly to the center of the head. However, the brainstem received 13.3 and 21.2 mGy for the isocenter located at 4 cm anterior and 4 cm posterior to the center of the head respectively.

Table 4. Thermoluminescent dosimeters (TLD) absorbed dose (mGy) of major organs at risk (OARs) in the head of the RANDO phantom delivered by the new 200° head-and-neck protocol with different isocenters

Organ	Position of isocenter		
	4 cm Anterior to center of head	Center of head	4 cm Posterior to center of head
Lens	12.99 ± 1.41	3.79 ± 0.10	2.58 ± 0.17
Retina	13.30 ± 1.67	9.01 ± 0.34	4.96 ± 0.49
Optic nerve	10.52 ± 0.34	10.48 ± 0.15	6.12 ± 0.53
Brainstem	13.34 ± 1.48	17.87 ± 0.29	21.19 ± 1.91
Spinal cord	18.59 ± 1.04	28.77 ± 0.23	29.72 ± 1.82

The organs irradiated by the pelvic scanning protocol were the bladder, gonad, colon, small intestine, bone marrow, rectum, and spinal cord. The absorbed dose of individual organ and the total effective dose of RANDO phantom irradiated by the new half-fan scanning protocol were about half of the old half-fan scanning protocol. The total effective doses from the new and old half-fan pelvic scanning protocols were 8.2 and 16.0 mSv, respectively. The total effective dose from the new half-fan pelvic scanning protocol was 51% of that from the old half-fan pelvic scanning protocol. This was because the exposure was only half for the new scanning protocol. With the new half-fan pelvic scanning protocol, the absorbed doses to bladder, bone surface, and rectum were 30.4, 20.8, and 22.8 mGy, respectively, whereas for the old pelvic scanning protocol the absorbed doses to bladder, bone surface, and rectum were 59.4, 40.8, and 46.5 mGy, respectively.

Image quality

Table 5 shows the summary of the results of image quality. For the head-and-neck scanning protocol, the low-contrast

resolutions for the new protocol (Fig. 1a) and old protocol (Fig. 1b) were 7 mm and 6 mm in diameter at 1% target contrast level, respectively. The 15 mm in diameter at 0.5% target contrast level could be detectable only for the old head-and-neck protocol, and was undetectable at 0.3% contrast level for both protocols. For the high-contrast spatial resolution, the new head-and-neck protocol (Fig. 2a) and old head-and-neck protocol (Fig. 2b) demonstrated the same resolution of 7 lp/cm.

Table 5. Summary of the image quality of different scanning protocols

	New (Version 1.4.13)	Old (Version 1.4.11)	New (Version 1.4.13)	Old (Version 1.4.11)
	Head	Head	Pelvis	Pelvis
Low-contrast				
Visible supra-slice target diameter (mm) at 1% target contrast level	7	6	7	6
Visible supra-slice target diameter (mm) at 0.5% target contrast level	Invisible	15	Invisible	15
Visible supraslice target diameter (mm) at 0.3% target contrast level	Invisible	Invisible	Invisible	Invisible
High-contrast spatial resolution (lp/cm)	7	7	4	5
Mean SD of CT numbers	13.1	8.6	6.1	6.0

Abbreviations: CT = computed tomography; SD = standard deviation.
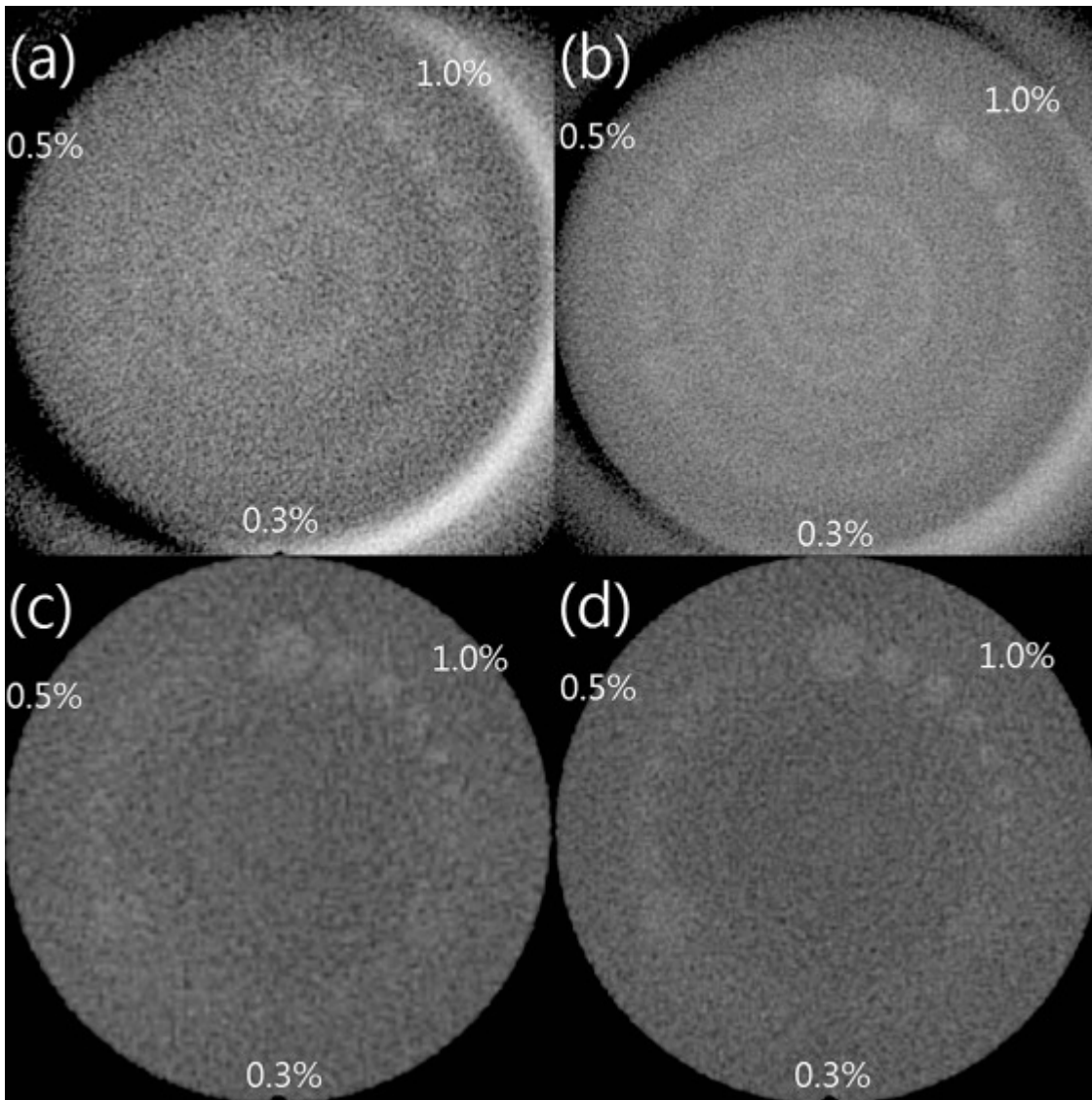
Fig. 1. Images of low-contrast resolution for (a) new head-and-neck protocol, (b) old head-and-neck protocol, (c) new pelvic protocol, and (d) old pelvic protocol. Display window, (200, 0) Hounsfield Unit (HU). Nominal target contrast levels are 0.3%, 0.5%, and 1.0%.
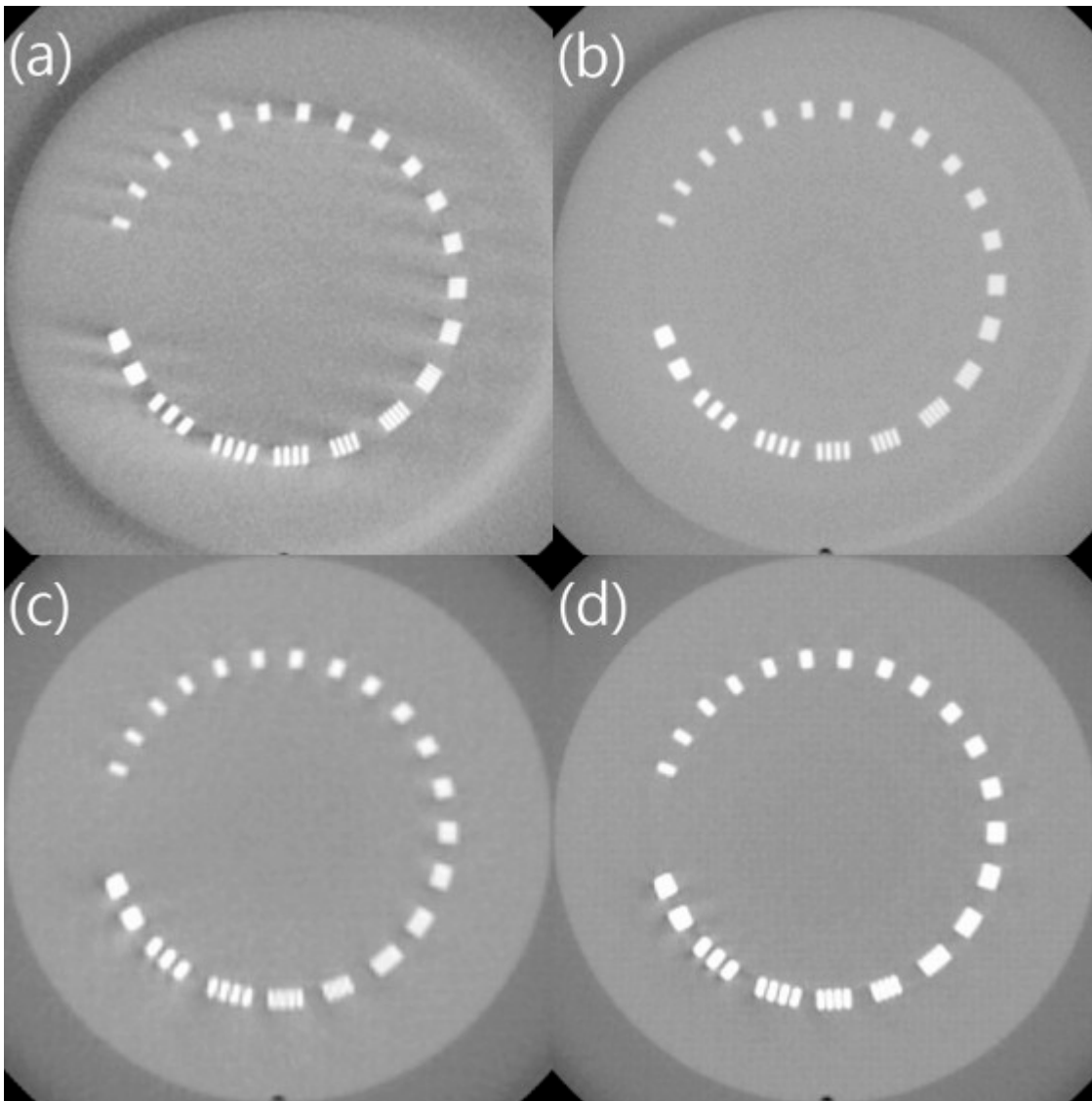
Fig. 2. Images of high-contrast spatial resolution for (a) new head-and-neck protocol, (b) old head-and-neck protocol, (c) new pelvic protocol, and (d) old pelvic protocol. Display window, (630, −300) Hounsfield Unit (HU).

The overall image quality for the old pelvic scanning protocol was found to be slightly better than that of the new pelvic protocol. The 1% of the low-contrast resolution for the new pelvic protocol (Fig. 1c) and old pelvic protocol (Fig. 1d) were 7 mm and 6 mm in diameter, respectively. The 15 mm in diameter at 0.5% target contrast level could be detectable only by the old pelvic protocol. The visibility of 0.3% target contrast level was not possible for both pelvic protocols. For the high-contrast spatial resolution, the new pelvic protocol (Fig. 2c) and old pelvic protocol (Fig. 2d) were able to resolve 4 and 5 lp/cm, respectively.

It should be noted that much image noise was found on the new head-and-neck protocol. However, the image noise was found similar on both pelvic protocols. To analyze the reconstructed images quantitatively, the CNRs of different inserts were found in the selected ROIs shown in Fig. 3. The CNR and FOM of different protocols are summarized in Table 6. To compare the CNR and FOM of different protocols, the average CNR and FOM were calculated from different inserts of each protocol. The better detectability of the low-contrast resolution for the old head-and-neck protocol was observed, revealing itself in an average CNR increased by a factor of 1.56 compared with the average CNR performed by the new head-and-neck protocol. The FOMs of the new and old head-and-neck protocols were 34.79 and 27.11, respectively. The

average values of the CNR for the new and old pelvic protocols were 68.66 and 49.34, respectively, and the FOMs were 335.98 and 80.78, respectively.
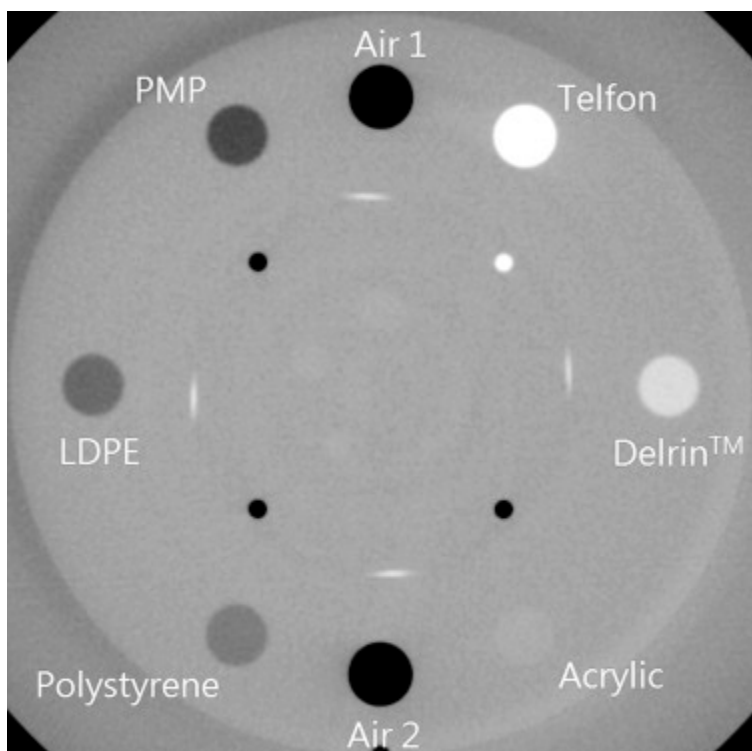

Fig. 3. Image reconstruction of the CTP404 module. The contrast inserts selected as regions of interest for the quantitative analysis of contrast-to-noise ratio (CNR) and figure of merit (FOM). Display window, (630, −300) Hounsfield Unit (HU).

Table 6. Contrast-to-noise ratio (CNR) and figure of merit (FOM) of new and old scanning protocols

| | New (Version 1.4.13) | | Old (Version 1.4.11) | | New (Version 1.4.13) | | Old (Version 1.4.11) | |
| | Head | | Head | | Pelvis | | Pelvis | |
	CNR	FOM	CNR	FOM	CNR	FOM	CNR	FOM
Polystyrene	6.38	1.11	10.50	0.94	12.69	5.48	10.69	1.96
LDPE	8.92	2.17	12.99	1.44	18.64	11.82	16.51	4.68
Air 1	63.95	111.72	102.30	89.60	186.33	1180.87	124.95	268.27
Air 2	65.01	115.47	101.54	88.28	184.84	1162.06	123.98	264.10
PMP	13.54	5.01	20.79	3.70	29.58	29.75	22.61	8.79
Acrylic	1.44	0.06	1.83	0.03	1.61	0.09	1.88	0.06
Delrin	10.33	2.92	13.55	1.57	25.56	22.23	21.53	7.96
Telfon	38.21	39.89	60.47	31.31	90.01	275.60	72.54	90.42
Average	25.97	34.79	40.50	27.11	68.66	335.98	49.34	80.78

Discussion

This study provided comprehensive information about absolute dosimetry of the new Varian CBCT protocols. Several researchers have reported the CBCTDI$_w$ using kV reference dosimetry. Song et al. found that the CBCTDI$_w$ for the

head-and-neck protocol of Elekta Synergy X-ray Volumetric Imager (XVI) system was 1 mGy at 100 kVp with 210° acquisition angle and that the CTDI at 0° was 1.3 mGy (18). For the Varian OBI system in this study, it was reported that the $CBCTDI_w$ of the old full-fan head-and-neck protocol was 116.8 mGy at 125 kVp with 360° acquisition angle and the CTDI at 0° was 116.1 mGy. The $CBCTDI_w$ for the new head-and-neck scanning protocol of the current study was 36.6 mGy, which was much higher than the Varian OBI system as reported by Palm et al.(34). This may be explained that Palm et al. used a narrow field to measure the $CBCTDI_w$ by reducing the blades (34). However, the energy of the current new head-and-neck protocol was lower than that of the old protocol. The CTDI at 0° position for the current new head-and-neck protocol was 12.9 mGy which was greatly reduced compared with the Varian old protocol. This was mainly due to the 200° scanning angle from 90° to 290°, and therefore the dose to the optic structures of a patient could be reduced. Kan et al. demonstrated that the absorbed dose of lens measured by TLD for the head-and-neck CBCT using standard mode was 62.2 mGy at 125 kVp with 360° acquisition angle (35). This dose was similar to the old head-and-neck protocol of the current study, which was 59.4 mGy. It should be noted that the lens dose of the new 200° scanning protocol was only 3.8 mGy. Therefore, the absorbed dose to the lens of a patient with head-and-neck cancer can be reduced by 1835 mGy if the patient was treated with 33 fractions with daily CBCT using new 200° head-and-neck protocol. The minimum cataractogenic dose for a protracted exposure of 3 weeks to 3 months is 4 Gy (36). It should be pointed out that the lens dose for many patients with advanced head-and-neck cancer, especially for superiorly extended NPC, may receive 5 to 6 Gy for the entire course of radiation treatment. Any additional dose from CBCT would further increase the chance of cataractogenesis. Using the blades to shield the lens during image guidance can effectively reduce additional radiation dose delivered to both lenses from CBCT if the region of eyeball is not essential for field matching. It was observed that the more posterior of the isocenter located, the less absorbed dose of the optic structures received. However, for the posteriorly located structures such as the brainstem and spinal cord, the absorbed dose was increased when the isocenter was located posteriorly.

The total effective doses from the new 200° and old 360° head-and-neck protocols were 1.7 mSv and 9.4 mSv, respectively. According to the ICRP 103, assuming a linear response at low doses, the combined detriment due to excess cancer and heritable effects remains at approximately 5% per Sv (27). When a patient with head-and-neck cancer received a daily CBCT for 33 fractions, the total effective doses from the new 200° and old 360° head-and-neck protocols would be 56.1 mSv and 310.2 mSv, respectively, which could induce additional secondary cancer risk of $2.8 \times 10{-}3$ and $15.5 \times 10{-}3$, respectively. The risk of inducing secondary cancer from the new 200° head-and-neck protocol was five times less than that of the old 360° head-and-neck protocol. A radical treatment of prostate cancer with 35 fractions daily CBCT for the new and old pelvic scans would result in additional effective doses of 287.4 mSv and 560.0 mSv, respectively, which could induce additional secondary cancer risks of 1.4% and 2.8%, respectively.

Uncertainties were introduced by using the anthropomorphic RANDO phantom in this study to measure the organ and total effective doses. It should be noted that the measurement of the organ and total effective doses in the phantom does not directly correspond to the real patient, as the effective atomic number and mass density of tissue and organ vary between the phantom and the human. Besides, there are uncertainties associated with the location of organs and the choice of TLD position within organs. These uncertainties are not easy to estimate quantitatively. Therefore, the measurement of the organ and total effective doses using this technique as a reliable basis for absolute risk estimation is inappropriate. However, it can be used to calculate the relative radiation risks of the patients who are receiving radiation from CBCT (37).

To compare the image quality of the head-and-neck protocols, the low-contrast resolution and CNR for the new protocol was poorer than those of the old protocol. However, both protocols demonstrated the same high-contrast spatial resolution. Both protocols were better than the vendor's recommended specifications of 15 mm at 1% supra-slice target diameter for the low-contrast resolution and 6 lp/cm for the high-contrast spatial resolution. Decreasing the tube voltage of the new head-and-neck protocol increased the image noise, which is shown in Table 5. It is complex to describe the relationship of tube voltage and image noise as it affects the production of photons via radiative stopping power in the tube and the photon attenuation via linear attenuation coefficient in the phantom (38). Nevertheless, the FOM results demonstrated that dose reduction can be achieved by reducing the tube voltage without much negative impact on CNR. In light of these findings, the image quality of the new head-and-neck protocol with lower radiation dose was acceptable because it was sufficient for image guidance using the "bone matching" method (17). The old pelvic protocol showed slightly better resolution on both tests of low-contrast and high-contrast spatial resolution. Both pelvic protocols demonstrated better image quality than the recommended specifications of 15 mm at 1% supra-slice target diameter for the low-contrast resolution. The high-contrast spatial resolution of the new pelvic protocol was not as high and just achieved the vendor's recommended specification of 4 lp/cm which is also acceptable for verification of isocenter by the method of bone matching. The CNR and FOM for the new pelvic protocols were higher than the old pelvic protocol. This can be explained by improving the reconstruction algorithms of the new protocol. Although the image quality of the new pelvic protocol was slightly worse than the old one, the radiation dose delivered by the new protocol was only one-half of the old protocol.

It should be noted that the low-contrast resolution perhaps was not adequate to identify the contour of soft tissue or tumor for all protocols. For example, it is not easy to localize the targets in the pelvic region such as prostate, bladder, cervix, and rectum on the images of CBCT because of the low detectability of low-contrast object. Therefore, the image-guided ART cannot be easily implemented because the position and the motion of these tumors are not totally correlated to the bony anatomy [39] and [40]. Improvement and further development on the low-contrast resolution of CBCT should be done to improve the visibility of soft tissues.

The new version of Varian CBCT offered good 3D images for image guidance with comparable image quality and lower radiation dose. Using the new protocols, the total effective dose delivered to patients was reduced and therefore the additional risk of inducing secondary risk due to the stochastic effect was also decreased.

Conclusion

This study has demonstrated that the new version of Varian CBCT offers a relatively low-dose 3D volumetric image registration on image guidance with comparable image quality. The dose measurement of CBCT using CT dosimetry and AAPM TG61 dosimetry protocol with the Farmer-type ionization chamber can be a standard for CBCT dosimetry. The lens dose for the new 200° head-and-neck protocol can be reduced from 59.4 to 3.8 mGy. It is obvious that the chance of inducing cataract can be decreased. The radiation dose increases with energy and mAs settings. For those patients who need daily CBCT for accurate treatment setup, the operator should consider to avoid employing higher energy and mAs if there is an alternative. All protocols provide sufficient 3D volumetric information of bony structure for the correction of geometric errors of the patient setup.

Further studies on the improvement of image quality of the CBCT with lower radiation dose will be useful. These results

lead us conclude that it is possible to perform routine CBCT for our clinical practice with minimum radiation dose.

References

1.   D.P. Dearnaley, V.S. Khoo, A.R. Norman et al. Comparison of radiation side-effects of conformal and conventional radiotherapy in prostate cancer: A randomized trial. Lancet, 353 (1999), pp. 267 – 271.

2.   M.J. Zelefsky, Z. Fuks, M. Hunt et al. High-dose intensity modulated radiation therapy for prostate cancer: Early toxicity and biochemical outcome in 772 patients. Int J Radiat Oncol Biol Phys, 53 (2002), pp. 1111 – 1116.

3.   A. Pollack, G.K. Zagars, L.G. Smith et al. Preliminary results of a randomized radiotherapy dose-escalation study comparing 70Gy with 78Gy for prostate cancer. J Clin Oncol, 18 (2000), pp. 3904 – 3911.

4.   P. Okunieff, D. Morgan, A. Niemierko, H.D. Suit. Radiation dose-response of human tumors. Int J Radiat Oncol Biol Phys, 32 (1995), pp. 1227 – 1237.

5.   D.A. Jaffray, D.G. Drake, M. Moreau et al. A radiographic and tomographic imaging system integrated into a medical linear accelerator for localization of bone and soft tissue targets. Int J Radiat Oncol Biol Phys, 45 (1999), pp. 773 – 789.

6.   A.L. Boyer, L. Antonuk, A. Fenster et al. A review of electronic portal imaging devices (EPIDs). Med Phys, 19 (1992), pp. 1 – 16.

7.   L. Pisani, D. Lockman, D. Jaffray et al. Set-up error in radiotherapy: On-line correction using electronic kilovoltage and megavoltage radiographs. Int J Radiat Oncol Biol Phys, 47 (2000), pp. 825 – 839.

8.   D.A. Jaffray, J.H. Siewerdsen. Cone-beam computed tomography with a flat-panel imager: Initial performance characterization. Med Phys, 27 (2000), pp. 1311 – 1323.

9.   D. Letourneau, J.W. Wong, M. Oldham et al. Cone-beam-CT guided radiation therapy: Technical implementation. Radiother Oncol, 75 (2005), pp. 279 – 286.

10. M. Oldham, D. Letourneau, L. Watt et al. Cone-beam-CT guided radiation therapy: A model for on-line application Radiother Oncol, 75 (2005), pp. 271 – 278.

11. L.A. Dawson, D.A. Jaffray. Advances in image-guided radiation therapy. J Clin Oncol, 25 (2007), pp. 938 – 946.

12. D.A. Jaffray, D.G. Drake, M. Moreau et al. A radiographic and tomographic imaging system integrated into a medical linear accelerator for localization of bone and soft-tissue targets. Int J Radiat Oncol Biol Phys, 45 (1999), pp. 773 – 789.

13. D.M. Duggan, G.X. Ding, C.W. Coffey et al. Deep-inspiration breath-hold kilovoltage conebeam CT for setup of stereotactic body radiation therapy for lung tumors: Initial experience. Lung Cancer, 56 (2007), pp. 77 – 88.

14. G.X. Ding, D.M. Duggan, C.W. Coffey et al. A study on adaptive IMRT treatment planning using kV cone-beam CT. Radiother Oncol, 85 (2007), pp. 116 – 125.

15. J.M. Schallenkamp, M.G. Herman, J.J. Kruse et al. Prostate position relative to pelvic bony anatomy based on intraprostatic gold markers and electronic portal imaging. Int J Radiat Oncol Biol Phys, 63 (2005), pp. 800 – 811.

16. International Commission on Radiation Units and Measurements. Pescribing, Recording and Reporting Photon Beam Therapy (Report 62). International Commission on Radiation Units and Measurements, Bethesda, MD (1999).

17. J.R. Sykes, A. Amer, J. Czajka et al. A feasibility study for image guided radiotherapy using low dose, high speed, cone beam X-ray volumetric imaging. Radiother Oncol, 77 (2005), pp. 45 – 52.

18. W.Y. Song, S. Kamath, S. Ozawa et al. A dose comparison study between XVI® and OBI® CBCT systems. Med Phys, 35 (2008), pp. 480 – 486.

19. P. Roxby, T. Kron, F. Foroudi et al. Simple methods to reduce patient dose in a Varian cone beam CT system for delivery verification in pelvic radiotherapy. Br J Radiol, 82 (2009), pp. 855 – 859.

20. B. Whiting, P. Massoumzadeh, J.O. Sullivan et al. The influence of bowtie filters on X-ray CT signals. Med Phys, 32 (2005), p. 2056.

21. J.T. Bushberg, J.A. Siebert, E.M. Leidholdt. The essential physics of medical imaging (2nd ed.)Lippincott Williams and Wilkins, Philadelphia (2002) p. 114.

22. C.M. Ma, C.W. Coffey, L.A. DeWerd et al. AAPM protocol for 40 – 300 kV x-ray beam dosimetry in radiotherapy and radiobiology. Med Phys, 28 (2001), pp. 868 – 893.

23. R. Fahrig, R. Dixon, T. Payne et al. Dose and image quality for a cone-beam C-arm CT system. Med Phys, 33 (2006), pp. 4541 – 4550.

24. L.J. Sawyer, S.A. Whittle, E.S. Matthews et al. Estimation of organs and effective doses resulting from cone beam CT imaging for radiotherapy treatment planning. Br J Radiol, 82 (2009), pp. 577 – 584.

25. A. Amer, T. Marchant, J. Sykes et al. Imaging doses from the Elekta Synergy X-ray cone beam CT system. Br J Radiol, 80 (2007), pp. 476 – 482.

26. A.J.J. Bos. High sensitivity thermoluminescence dosimetry. Nucl Instrum Methods Phys Res B, 184 (2001), pp. 3 – 28.

27. ICRP 103. The 2007 recommendations of the International Commission on Radiological Protection Publication 103. Annals of ICRP, 37 (2007), pp. 1 – 332.

28. M. Stock, M. Pasler, W. Birkfellner et al. Image quality and stability of image-guided radiotherapy (IGRT) devices: A comparative study. Radiother Oncol, 93 (2009), pp. 1 – 7.

29. J. Stützel, U. Oelfke, S. Nill. A quantitative image quality comparison of four different image guided radiotherapy devices. Radiother Oncol, 86 (2008), pp. 20 – 24.

30. O. Morin, J.F. Aubry, M. Aubin et al. Physical performance and image optimization of megavoltage cone-beam CT. Med Phys, 36 (2009), pp. 1421 – 1432.

31. J. Wong, T. Xu, A. Husain et al. Effect of area x-ray beam equalization on image quality and dose in digital mammography. Phys Med Biol, 49 (2004), pp. 3539 – 3557.

32. Z. Szucs-Farkas, F.R. Verdun, G. von Allmen et al. Effect of X-ray tube parameters, iodine concentration, and patient size on image quality in pulmonary computed tomography angiography: A chest-phantom-study. Invest Radiol, 43 (2008), pp. 374 – 381.

33. C.J. Lai, L. Chen, H. Zhang et al. Reduction in x-ray scatter and radiation dose for volume-of-interest (VOI) cone beam breast CT—a phantom study. Phys Med Biol, 54 (2009), pp. 6691 – 6709.

34. A. Palm, E. Nilsson, L. Herrnsdorf. Absorbed dose and dose rate using the Varian OBI 1.3 and 1.4 CBCT system. J Appl Clin Med Phys, 11 (2010), pp. 229 – 240.

35. M.W.K. Kan, L.H.T. Leung, W. Wong et al. Radiation dose from cone beam computed tomography for image-guided radiation therapy. Int J Radiat Oncol Biol Phys, 70 (2008), pp. 272 – 279.

36. E.J. Hall, A.J. Giaccia. Radiobiology for the radiologist. (6th edition)Lippincott, Williams, & Wilkins, Philadelphia, PA (2006) p. 185.

37. R.M. Harrison, M. Wilkinson, A. Shemilt et al. Organ doses from prostate radiotherapy and associated concomitant exposures. Br J Radiol, 79 (2006), pp. 487 – 496.

38. M. Hilts, C. Duzenli. Image noise in X-ray CT polymer gel dosimetry. J Phys Conf Ser, 3 (2004), pp. 252 – 256.

39. F.J. Pos, M. Hulshof, J. Lebesque et al. Adaptive radiotherapy for invasive bladder cancer: A feasibility study. Int J Radiat Oncol Biol Phys, 64 (2006), pp. 862 – 868.

40. J.M. Schallenkamp, M.G. Herman, J.J. Kruse et al. Prostate position relative to pelvic bony anatomy based on intraprostatic gold markers electronic portal imaging. Int J Radiat Oncol Biol Phys, 63 (2005), pp. 800 – 811.

Conflict of interest: none.

Reprint requests to: Dora Kwong, M.D., Department of Clinical Oncology, University of Hong Kong, 1/F, Professorial Block, Queen Mary Hospital, Pokfulam, Hong Kong SAR, China. Tel: (+852) 2255-4521; Fax: (+852) 2872-6426